ACADEMIC PRESS

Available online at www.sciencedirect.com

SCIENCE DIRECT®

NeuroImage 18 (2003) 595–609

NeuroImage

www.elsevier.com/locate/ynimg

Consistent and precise localization of brain activity in human primary visual cortex by MEG and fMRI

F. Moradi,[a] L.C. Liu,[a] K. Cheng,[b] R.A. Waggoner,[b] K. Tanaka,[b] and A.A. Ioannides[a,*]

[a] *Laboratory for Human Brain Dynamics, RIKEN Brain Science Institute (BSI), Wako-Shi, Saitama 351-0198, Japan*
[b] *Laboratory for Cognitive Brain Mapping, RIKEN Brain Science Institute (BSI), Wako-Shi, Saitama 351-0198, Japan*

Received 19 March 2002; revised 3 October 2002; accepted 14 October 2002

Abstract

The tomographic localization of activity within human primary visual cortex (striate cortex or V1) was examined using whole-head magnetoencephalography (MEG) and 4-T functional magnetic resonance imaging (fMRI) in four subjects. Circular checkerboard pattern stimuli with radii from 1.8 to 5.2° were presented at eccentricity of 8° and angular position of 45° in the lower quadrant of the visual field to excite the dorsal part of V1 which is distant from the V1/V2 border and from the fundus of the calcarine sulcus. Both fMRI and MEG identified spatially well-overlapped activity within the targeted area in each subject. For MEG, in three subjects a very precise activation in V1 was identified at 42 ms for at least one of the two larger stimulus sizes (radii 4.5 and 5.2°). When this V1 activity was present, it marked the beginning of a weak wave of excitations in striate and extrastriate areas which ended at 50 ms (M50). The beginning of the next wave of activations (M70) was also marked by a brief V1 activation, mainly between 50 and 60 ms. The mean separation between V1 activation centers identified by fMRI and the earliest MEG activation was 3–5 mm.

Keywords: Magnetoencephalography (MEG); Functional magnetic resonance imaging (fMRI); Primary visual cortex (striate cortex or V1); Visual evoked field; Magnetic field tomography (MFT); Human

Introduction

Most of our data about localization and retinotopic organization of the primary visual cortex (striate cortex or V1) in humans come from lesion studies (Horton and Hoyt, 1991), functional imaging with positron emission tomography (PET) (Fox et al., 1987), and functional magnetic resonance imaging (fMRI) (DeYoe et al., 1996; Engel et al., 1997; Sereno et al., 1995). Localization accuracy and resolution of fMRI underwent rapid advancement in the past decade. Recent studies aimed successfully at submillimeter structures such as ocular dominance columns in humans (Cheng et al., 2001; Menon et al., 1997; Menon and Goodyear, 1999) and orientation columns in cat's visual cortex (Kim et al., 2000). However, the temporal resolution of PET and fMRI and other similar techniques that depend on slow metabolic changes that accompany neuronal activity rather than the neuronal activity directly is not enough to study the dynamics that govern the activation of different brain areas (Ogawa et al., 1998). Magnetoencephalography (MEG) is a noninvasive technique that directly measures mass postsynaptic neuronal potentials (Hamalainen et al., 1993) with excellent native temporal resolution. However, the localization of MEG has been the subject of intense study and, at times, controversy, partly because no "gold standard" for comparison is available in normal human brains.

Primary visual cortex offers a precise testing ground to study the limits of each technique and to compare electromagnetic and metabolic sources with respect to the known retinotopic organization of V1. The standard cruciform model (Okada 1983; Onofrj et al., 1995) was only partially supported by source estimation from visually evoked electromagnetographic (EEG) data (Ahlfors et al., 1992; Maclin

* Corresponding author. Laboratory for Human Brain Dynamics, RIKEN Brain Science Institute (BSI), 2-1 Hirosawa, Wako-shi, Saitama 351-0198, Japan. Fax: +81-48-467-9731.

E-mail address: ioannides@postman.riken.go.jp (A.A. Ioannides).

1053-8119/03/$ – see front matter © 2003 Elsevier Science (USA). All rights reserved.
doi:10.1016/S1053-8119(02)00053-8

et al., 1983; Nakamura et al., 1997; Slotnick et al., 1999). The results were often inconsistent with the known retinotopic organization (Aine et al., 1996; Onofrj et al., 1995). Direct comparison between electromagnetic and metabolic methods provides, at a first glance, an ideal combination. Many such recent studies met with limited success, reporting dipole sources estimated from either EEG or MEG measurements to be one to several centimeters away from the fMRI activation loci in V1 (Beisteiner et al., 1997; Disbrow et al., 2000; Eulitz et al., 1994; Gratton et al., 1997; Roberts et al., 2000; Stippich et al., 1998). The discrepancies were attributed either to technical problems with MEG or fMRI, or to the ambiguity of biomagnetic inverse solutions, but they may simply reflect fundamentally different hemodynamic and electrophysiological processes (Bonmassar et al., 2001; Nunez and Silberstein, 2000) and the fact that each probes very different time scales (Ioannides, 1999). On the other hand, increased neuronal activity that occurs with reduced firing synchrony may not produce detectable scalp electric or magnetic fields. Another possible contribution to the difference is the way solutions are calculated. The current dipole model is often used for MEG and EEG, thus reducing the activity to one or a few point-like sources computed from average data. We have recently demonstrated that localization with accurate retinotopy is easier to achieve with distributed source analysis and specifically magnetic field tomography (MFT) (Ioannides, 1994; Ioannides et al., 1990) rather than with equivalent current dipoles because of the presence of early but labile activity in extrastriate areas (Tzelepi et al., 2001). The presence of early activation in extrastriate areas, was also demonstrated in another MEG study using distributed source analysis, but no comparison with current dipole solutions was presented (Vanni et al., 2001). In both studies activity was identified in a number of extrastriate areas, and prominently in two such areas. The first area had temporo-occipital location, consistent with the V5/MT area. The second area was in the parieto-occipital sulcus and its activation was interpreted both in the two recent MEG studies and in an earlier MEG study using current dipole analysis (Portin et al., 1999) as the human homologue of the monkey area V6 (Gallettii et al., 1999). For ease of reference we will label this area putative V6.

PET and fMRI solutions are expressed tomographically as statistical parametric maps. What is required for a better comparison is to add statistical analysis to the MFT solutions and to compare the results with established fMRI statistical tomographic solutions. It is further desirable to have a third, even approximate but independent measure of where the expected V1 activation should be, so that it is clearly discriminated from activations in areas beyond V1, such as V2/V3. This work targeted these goals, following logically from two previous investigations where we studied completely independently the localization of fMRI (Cheng et al., 2001) and MEG (Tzelepi et al., 2001). Identical reversing checkerboard patterns were used in both techniques, but with the flickering frequency optimized for each technique based on signal-to-noise ratio (SNR) measurements from a pilot experiment and other studies (Singh et al., 2000; Thomas and Menon, 1998). For the analysis, we used similar techniques to extract tomographic statistical estimates from fMRI and MEG data. The results were compared to each other, and to the expected location derived from a separate fMRI retinotopy experiment, without any assumptions about mechanisms of electromagnetic and metabolic activation or the nature and number of generators. Finally we repeated the fMRI main experiment with one of the subjects using the two flickering frequencies in the respective MEG and fMRI experiments, confirming that the fMRI localization in V1 was nearly identical for the two flickering frequencies.

Materials and methods

Subjects and stimuli

Four male subjects (ages 27–35) from RIKEN Brain Science Institute with normal or corrected to normal visual acuity participated in the experiments, which were approved by the RIKEN functional MRI safety and institutional ethical committees. The procedure and scientific background for the experiments were fully explained to each subject and a signed agreement for participation was obtained prior to the experiments. Stimuli consisted of flickering (reversing) checkerboard patterns on a homogenous gray background: check size of 1°, 45° orientation, 8° from a fixation point (a small red cross at the center of the screen) along the downward diagonal in left (subjects 1 and 3) or right (subjects 2 and 4) lower visual quadrant, radii of 1.8, 2.6, 3.7, 4.5, and 5.2°. For subjects 2 and 4 two additional smaller radii of 1.0 and 1.5° were also used. The fMRI experiment was conducted with an 8-Hz flickering frequency (125 ms between cycles). For MEG we used a lower flickering frequency of 0.71 Hz (1400 ms between cycles) to limit interference from successive stimuli. Thomas and Menon (1998) have reported that the location of the blood oxygenation level dependent (BOLD) response to flickering stimuli is consistent from 0.5 to 31.25 Hz (the range tested); thus the fMRI results should be directly comparable with the MEG results. We have nevertheless confirmed this expectation by running a new fMRI experiment, after completing the analysis of both fMRI and MEG data. Specifically, we repeated the fMRI experiment for subject 2 with the stimulus radius that gave the best results in MEG (4.5°) using the two flickering frequencies (8 and 0.71 Hz) in separate blocks.

Different sizes were tested in separate runs within a single experimental session for each modality. The order of the runs was always from the smallest to the largest stimulus. During the control period in the fMRI recording and subject baseline runs in the MEG recording, only the fixation cross on the homogenous gray background (same as in

the stimulation) was presented. The subjects were instructed to fixate on the cross during the whole experiment.

Stimulation apparatus

The stimuli were presented to the subjects' eyes via two fiber optic bundles from LCD displays (Avotec, Inc., Jensen Beach, FL) with the subjects at supine position. The visual field was 30 × 23°. The contrast of the stimulus was 84% (black 0.05 cd/m^2, white 0.59 cd/m^2, gray 0.28 cd/m^2). For the MEG experiment, reversals were synchronized with the vertical rescan signal generated by the graphic adapter of the computer.

fMRI acquisition

The fMRI experiment was conducted using a Varian Unity Inova 4-T whole-body MRI system (Varian NMR Instruments, Palo Alto, CA) with a butterfly quadrature radiofrequency (RF) surface coil. During the recording, the subject's head was fixed using a bite bar. Two pressure sensors were also placed around the subject's head to monitor any head motion. Before the main experiment, two preliminary fMRI experiments were conducted for each subject to determine the optimal location and orientation of slices. First, vertical and horizontal meridian stimulation was performed to identify borders between different visual areas. Second, four flickering checkerboard rings with different sizes (radius of 0–1.25°, 1.25–2.5°, 2.5–5°, and 5–10°) were used to sketch a coarse retinotopic (eccentricity) map of each subject on slices parallel to the calcarine sulcus. More details of the preliminary experiments can be found elsewhere (Cheng et al., 2001).

For most individuals, the cortical surface around the calcarine sulcus has a distinct morphology that can be very asymmetric between the left and right hemispheres and between the dorsal and the ventral parts of each hemisphere. Our visual stimulation apparatus limited the visual field to the central 20°. The visual field quadrant to be stimulated in the main experiment was selected individually for each subject so that the available visual field (excluding the foveal region up to ~3°) corresponded to a relatively smooth portion of the dorsal V1 for that subject.

For the main functional experiment, multishot T2*-weighted echo-planar imaging (EPI) was used (TR = 8.8 s, TE = 25 ms; the average flip angle for the RF excitation over the area of interest was approximately 45°). The images were acquired in 16 segments to minimize distortions. Interleaving and navigator echo correction (Hu and Kim, 1994) were used to maximize SNR and minimize segmentation artifacts. Each EPI volume consisted of six oblique slices parallel to the contralateral calcarine sulcus. The six-slice volume started at the inferior lip of the calcarine sulcus, extending dorsally through the lower and upper banks of the calcarine sulcus through the superior lip and the medial wall up to the dorsal V1/V2 border and some part of the dorsal V2. The slice thickness was 4 mm for subject 1 and 3 mm for the other three subjects. The in-plane resolution was 0.9×0.9 mm^2. Three cycles of control and stimulation were repeated. In total, 60 volumes over 528 s were scanned. Before individual functional scans, T1-weighted anatomical scans with an inversion recovery FLASH pulse sequence were taken at the same slice positions.

The cardiac cycle of the subject was recorded using an infrared pulseoxymeter. Respiration was also recorded simultaneously during the experiment. These data were used to correct signal changes correlated with cardiac and respiratory cycles (Hu et al., 1995). The data were corrected for time series baseline drifts using a zero-frequency notch filter. Each slice was corrected for in-plane head motions (Maas et al., 1997). The first volume for each condition (8.8 s from the stimulation onset or control periods) was excluded in the statistical analysis. To reduce spatial noise, a Gaussian filter with a FWHM of 1.8 mm was applied to the functional data. FMRI data were analyzed using the software package STIMULATE (Strupp, 1996). A one-tailed Student t test was then performed to identify significantly activated voxels during the stimulation versus the control periods. Dedicated software was developed to extract automatically contours from the STIMULATE output corresponding to predefined statistical significance threshold and

Fig. 1. Placement of fMRI slices relative to the V1/V2 border for subject 2. (A) Placement of the six paracalcarine slices used in main experiment and their relation to the V1/V2 border (blue squares) and calcarine sulcus (CS). Slices 3-3′ and 4-4′ and some part of slice 5-5′ cover the dorsal V1 on the left hemisphere. The representation of V1/V2 border is not clear on the foveal part of V1. (B) Vertical meridian stimulation activates areas close to the border of V1 and V2. The activated area is shown on a cut perpendicular to the CS (slice b-b′ as indicated in (A)). Blue arrows indicate V1/V2 borders on the left hemisphere. (C) Same as (B) but for slice c-c′ as indicated in (A).

Fig. 2. Retinotopic organization as revealed by fMRI for subject 2. (A) Borders of activated areas for flickering checkerboard rings with different diameters for slice 3 (Fig. 1A). The 0–2.5° ring that stimulated foveal part of the visual field is projected mostly on the occipital pole (red contours). As the eccentricity of the stimulus increases the activation moves medially toward the lip of the calcarine and then along the calcarine in a posterior to anterior direction. The white circle marks the estimate for the targeted area based on the succession of maps with different eccentricity. Considering the placement of slices relative to calcarine and V1/V2 border (Fig. 1A), the V1 activation by the stimulus in the lower right visual field will be in slices 3 to 5 (Fig. 1A). (B) Same as (A) but for slice 4 as indicated in Fig. 1A. (C) Same as (A) but for slice 5 as indicated in Fig. 1A. Dashed rectangles mark the shown area for (D–F). (D) Different sizes of flickering checkerboard pattern with same eccentricity (center of checkerboard disk to fixation spot = 8°) were used to stimulate the targeted area. Borders of activated area for each stimulus is shown with different colors for the activations in the slice similar to that shown in (A). (E) As (D) for the slice similar to that shown in (B). (F) As (D) for the slice similar to that shown in (C). Contours correspond to activated areas of maps with $P < 0.01$. The set of contours highlighted by a white arrow is in V2.

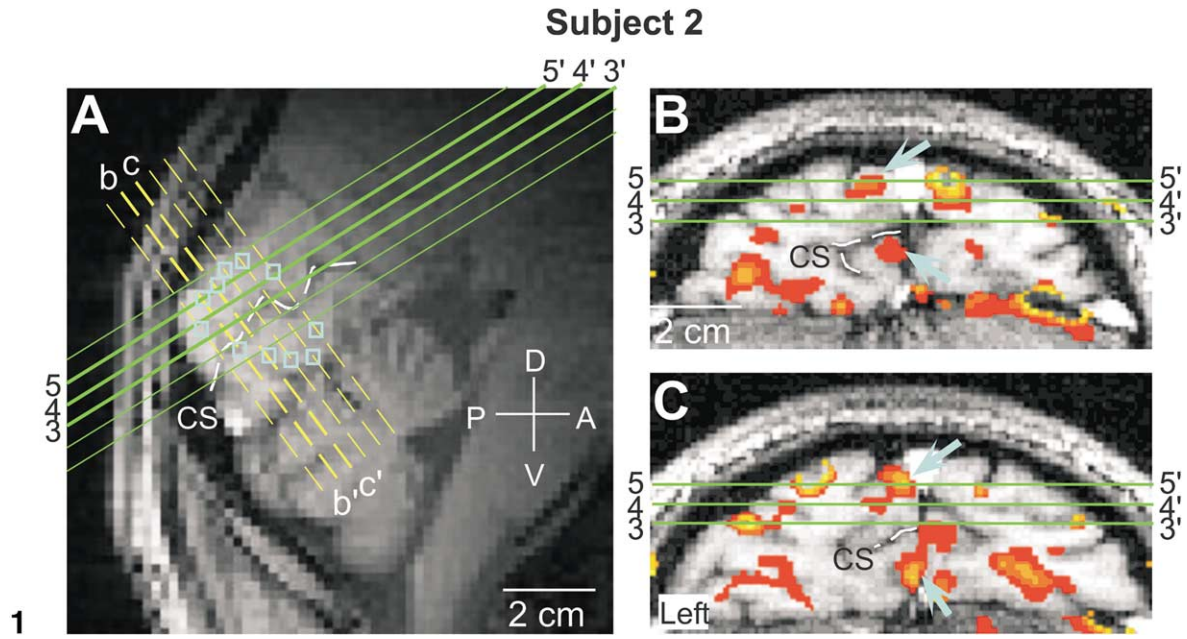
Subject 2
5' 4' 3'
A
b c
CS
5
4
3
D
P
A
V
b' c'
2 cm
B
5
4
3
5'
4'
3'
CS
2 cm
C
5
4
3
5'
4'
3'
CS
Left
1

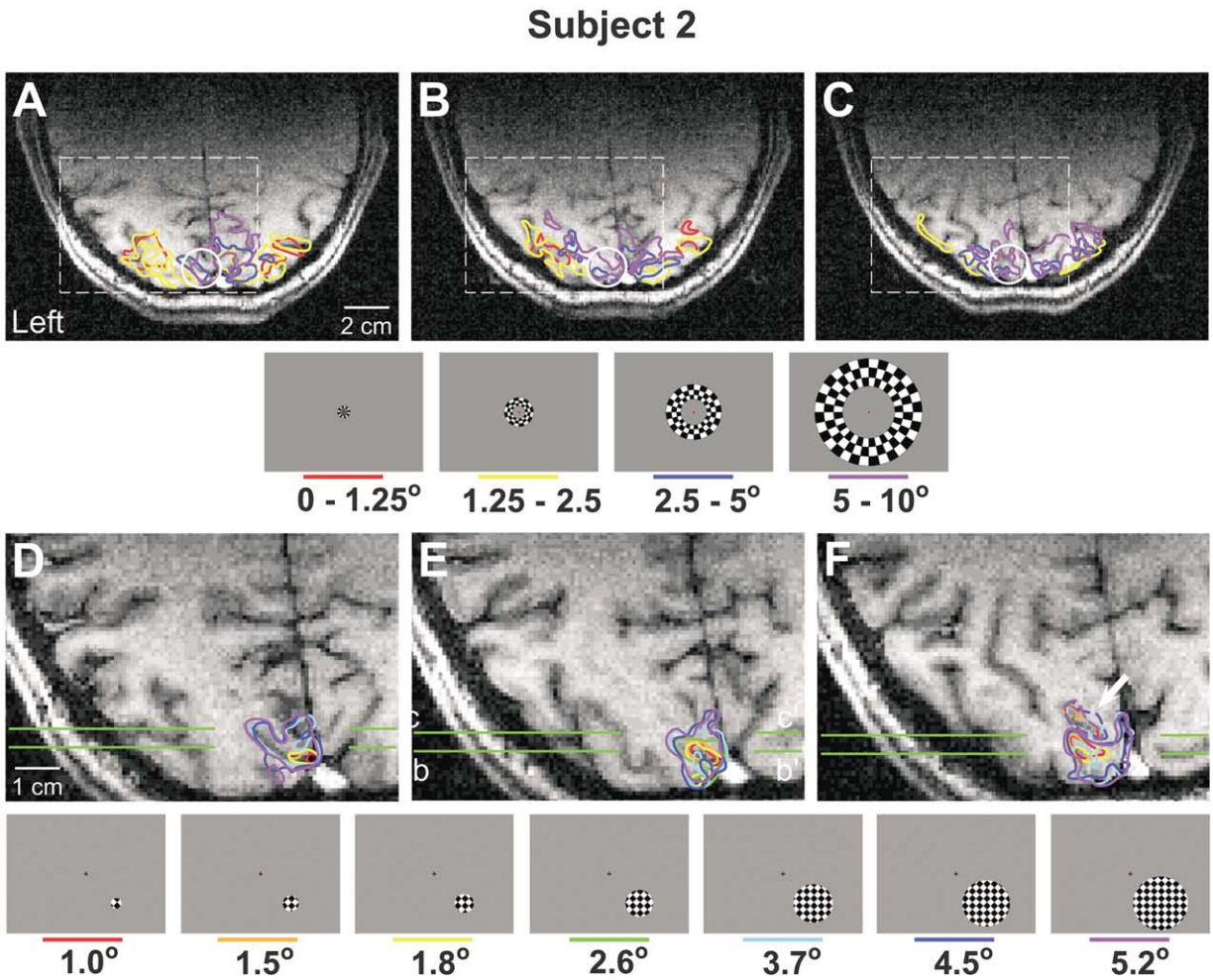
Subject 2
A
Left
2 cm
B
C
0 - 1.25°
1.25 - 2.5
2.5 - 5°
5 - 10°
D
1 cm
E
c
b
c'
b'
F
1.0°
1.5°
1.8°
2.6°
3.7°
4.5°
5.2°
2

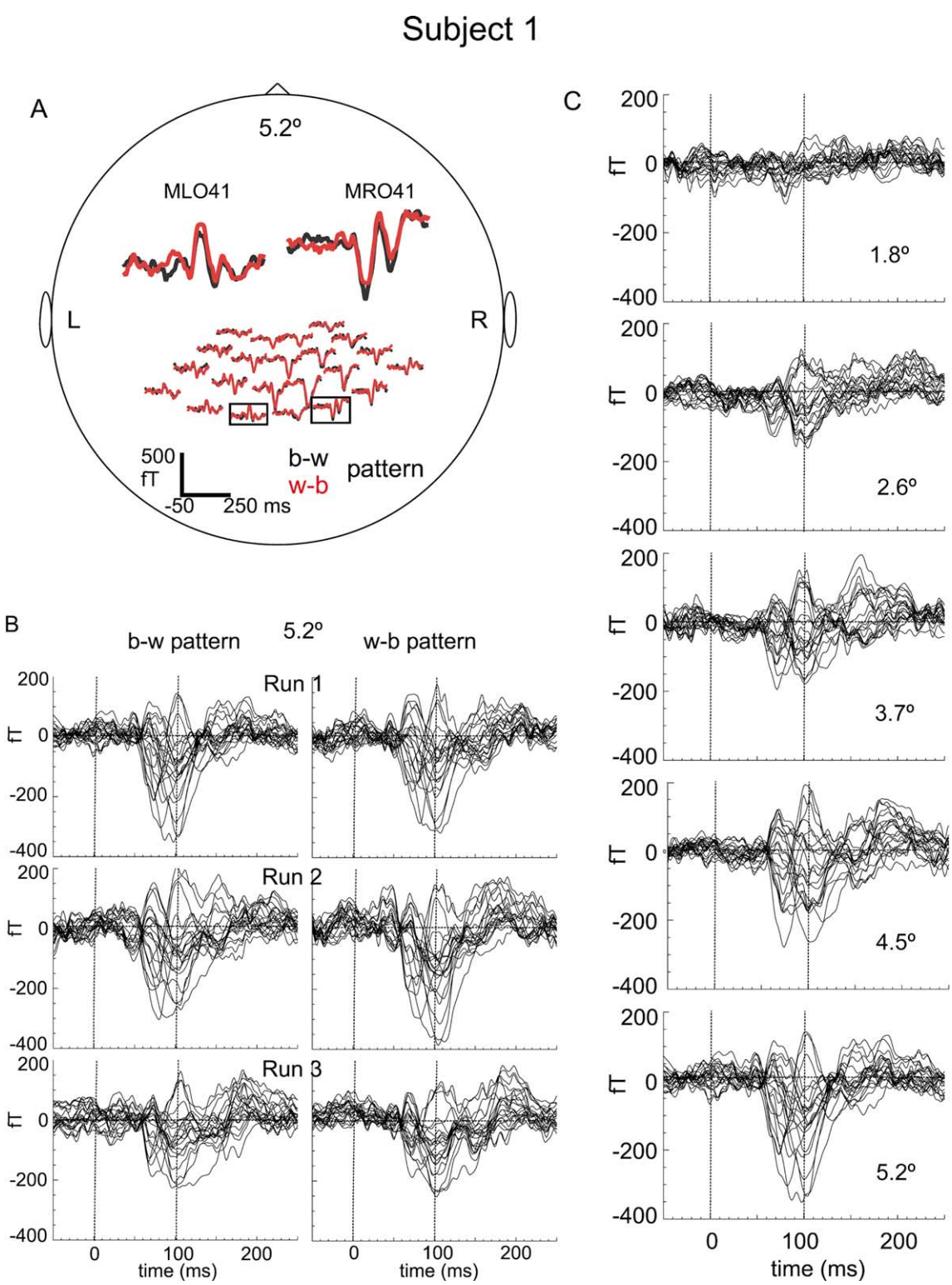

Fig. 3. Averaged MEG signal for subject 1 with stimuli presented on the lower left quadrant of the screen. The averaged signal was computed over ~100 trials. The signals from the 22 MEG channels covering the subject's occipital area were plotted from −50 to 250 ms relative to the pattern onset. (A) The MEG signals from the two patterns (black to white, b-w pattern; and white to black, w-b pattern) of stimulus size 5.2° in run 1 were superimposed channel by channel. The black and red curves denote the b-w and w-b pattern, respectively. The two occipital channels (MLO41 and MRO41) with the strongest signal of opposite polarity are highlighted by small black boxes and their magnified traces of signals are printed separately. The signal distribution is consistent with the presence of a focal source between these two occipital channels. (B) The average signal from each of 6 averages for size 5.2° was plotted in each figurine with the signals from the 22 channels superimposed together. (C) Changes in the signal with stimulus size for the average signals from the w-b pattern in run 1 of size 1.8–5.2°.

the percentage increase in activity, and superimpose them to the anatomical map of the subject. For each subject, two maps were produced for each stimulus size, at significance levels 0.001 and 0.005, respectively. Voxels with a percentage signal change 10% or higher were removed from each map because they were associated with large venous vessels (Gati et al., 1997; Luh et al., 2000; Cheng et al., 2001).

MEG recording

The MEG signal was recorded with the whole-head Omega biomagnetometer (CTF Systems, Inc., Vancouver, B.C., Canada) inside a magnetically shielded room (NKK, Japan). During the experiment, 151 MEG and 28 reference channels were recorded simultaneously together with horizontal and vertical electrooculogram (EOG) and four pairs of electrocardiogram (ECG) electrodes. Each MEG channel is a first-order axial gradiometer with two 1-cm radius coils separated by 5 cm. The subjects rested the back of their head on the helmet so the distance between the occipital part of the brain and MEG sensors was minimized.

The MEG data were recorded continuously with a sampling rate of 625 Hz after low pass filtering at 200 Hz. Each run consisted of 30 s gray screen with the fixation cross and 240 trials of black to white b-w and white to black w-b patterns (120 trials for each pattern). Three runs for each stimulus size were recorded. Two subject baseline runs were also recorded, one before and one after the stimulation runs. In these two runs, the subjects were in place with the same luminosity and fixation cross on the screen as in the stimulation runs.

Environmental noise was first eliminated by forming the third gradient of the magnetic field off-line and the resulting data were further bandpass-filtered in the 1- to 120-Hz range with notch filters at 50 and 100 Hz. The ECG artifact was then removed using a noise cancellation technique based on the correlation of recorded ECG and MEG signals. Trials were extracted from -100 to 400 ms relative to the onset of each pattern reversal (each pattern lasted for 700 ms). Trials with blinks or eye movements (changes greater than 50 μV in the EOG channels for subjects 1–3, 100 μV for subject 4) were automatically removed. On average about 20% of the trials were removed because of the subject artifacts. The remaining trials were averaged separately for each pattern in each run, resulting in six averages of $\sim$100 trials per stimulus size for each subject.

Coregistrations of MEG and MRI

High resolution anatomical images of the subjects were taken with a 1.5-T Siemens Magneton Symphony system. For each subject, T1-weighted MRI images (voxel size of $1\times1\times1$ mm^3) were collected. Before the MEG experiment, three head coils were attached to the subject's scalp, close to the nasion, the left and the right preauricular points, respectively. The three coils defined a coordinate system (coil coordinate system). The subject's head shape was scanned using a 3D digitizer (Polhemus, 3Space/Fastrak, USA). The digitized head shape was fitted on the MRI to get a transformation matrix between coil and MRI coordinate systems using a dedicated in-house software. The results for the coregistration were checked manually, and if the fit was not accurate, the digitization process was repeated. Before and after each recording run, the subject's head position was monitored with the three head coils. If a subject had moved excessively during a run (4 mm or more) that run was repeated.

A second coregistration was made between the 4- and 1.5-T anatomical MRI images. In-house software was developed to allow the matching of points and outlines in the two sets of images and hence to coregister the six-slice volume from the 4-T with the full volume from the 1.5-T MRI. The fMRI/MEG results are displayed on the 1.5-T anatomical images that match each one of the six slices used for the main fMRI acquisition.

Distributed source analysis

MFT (Ioannides, 1994; Ioannides et al., 1990) was applied to the averaged data (stimulation and baseline runs) to produce probabilistic estimates for the nonsilent primary current density vector $\mathbf{J}(\mathbf{r},t)$ from -100 to 400 ms relative to the onset of each pattern at steps of 1.6 ms. The MFT algorithm relies on a nonlinear solution to the inverse problem, where the sensitivity profile of the sensors is used as an expansion basis for the direction of the primary current density MFT (Ioannides et al., 1990). A weighted expansion is used, with the a priori probability weight determined through a training session from computer-generated data. For each experimental arrangement (i.e., for each run and subject) a different a priori probability weight is used, determined by a separate training session. The training with the computer generated data fixes the only two free parameters (regularization and a priori probability weight) before the real data are processed (Ioannides, 1994). The analysis of the real data then proceeds time slice by time slice with all free parameters fixed. The heavy computational cost associated with the solution of a nonlinear system for each time slice is accepted because the nonlinearity of the method exploits optimally the moment by moment information in the spatial distribution of signal values in the sensor array (Taylor et al., 1999). For each subject, four hemispherical source spaces were defined, each covering the left, right, top, and back part of the brain well. MFT was then used separately to extract brain activity from the MEG signal corresponding to the 90 channels closest to each of the four source spaces. The spatially overlapping estimates from the four source spaces were combined into one covering the entire brain. The algorithmic steps and mathematical details of the method can be found elsewhere (Ioannides 1994; Ioannides et al., 1990; Taylor et al., 1999). Validation of the method with computer-generated data and the anal-

ysis average data can be found in the early applications using the method (Ioannides et al., 1990, 1993b; Ribary et al., 1991), including comparison with implanted dipoles in humans (Ioannides et al., 1993a). Recent studies have focused on single-trial analysis, and for a review see Ioannides (2001).

The time course of regional activations is studied by computing the mean current density within a circumscribed 3D region of interest (ROI). In our study we first identified foci of maximal activity in the average signal and defined ROIs as spheres centered around each foci with radii of 8 mm. Each ROI was then labeled according to anatomical location. For each of the six runs corresponding to the same stimulus size, an ROI activation curve, $J_1(t)$, was calculated along the main direction of the current density as a function of time, where $J_1(t) = \int_{\mathrm{ROI}} \mathbf{J}(\mathbf{r},t)\cdot\hat{\mathbf{u}}_{\mathrm{ROI}}\, d^3\mathbf{r}$, with $\hat{\mathbf{u}}_{\mathrm{ROI}}$ the direction of the current density vector at the maximum (modulus) of the MFT activation. In this article, we will discuss only the results of the analysis of the ROI sampling activity from the V1/V2 area, and specifically the average and SNR computed across the repetitions corresponding to the same stimulus size.

Post-MFT statistical analysis

The MFT estimates for each time slice were smoothed by averaging the current density vector over a 6.4-ms window. For each stimulus size (three runs, two patterns in each run), the modulus of the smoothed current density from the six averages was the basic unit (element) for the statistical analysis; i.e., each time slice of each stimulus size was characterized by the "active" distribution of its 6 elements. For some cases one of the three runs either was corrupted by noise or had very weak responses, leaving a distribution with only four elements. Fatigue and associated small movement may be a reason for the weak signal in the excluded runs, supported by a relatively large difference between the coordinates of the three head coils at the beginning and end of these runs. Typically the head-coil discrepancy between the localizations made at the beginning and end of a run was about 1 mm, but for most of the excluded runs it was 2 mm or higher. For the control conditions, three baseline distributions were made for the activation in the absence of a stimulus each corresponding to distributions with 60 elements, 30 from each subject baseline run. The elements in the subject baseline distribution were selected randomly from the whole period (-100 to 400 ms), but with at least a 10-ms separation between elements. A paired t test was made between distributions from each target (6 elements) and each of the three baselines (60 elements). The least significant comparison (highest P value, corrected for multiple voxel comparisons) was assigned to the target window. On completion of these operations a signed P value was computed for each voxel, at each time slice of each stimulus size for each subject. This value corresponded to the confidence level for rejecting the null hypothesis of no significant increase (positive P value) or decrease (negative P value) of activity in the MFT estimates between the active and the control distributions.

Results

fMRI results

In all four subjects, the V1/V2 borders were identified by mapping the representation of the vertical meridian (Fig. 1). The representation of the horizontal meridian was located in the depth of the calcarine sulcus. Most of the V1 was buried inside the calcarine sulcus. Checkerboard rings of four different sizes were used to trace the activation at different eccentricities (Figs. 2A–2C). For each subject, the changes in activity with eccentricity were consistent with the known retinotopic structure of V1 (DeYoe et al., 1996; Engel et al., 1997; Fox et al., 1987; Horton and Hoyt, 1991; Sereno et al., 1995). The fMRI activations showing the cortical representation of the four ring stimuli of different sizes and that of vertical and horizontal meridians were visually examined to determine the V1 excitation for each subject. The target quadrant selected was the one activating the largest portion of V1 on the medial wall. This quadrant was endowed with the best separation between the central V1 representation, the V1/V2 border, and the fundus of the calcarine sulcus. The selected quadrants were all in the lower visual field, represented by the dorsal V1, on the right hemisphere in subjects 1 and 3, and on the left hemisphere in subjects 2 and 4.

For the main fMRI experiment we used stimuli centered along the diagonal bisecting the selected lower quadrant at 8° eccentricity. The targeted area was therefore 8° away from the foveal representation and midway between the representation of the horizontal meridian and that of the vertical meridian (i.e., the dorsal V1/V2 border). As expected, the V1 activation was localized in the upper bank of the contralateral calcarine and/or the superior lip of the calcarine sulcus on the medial wall (Fig. 2). The eccentricity of the activation site matched the results obtained in the eccentricity experiment with checkerboard rings of different sizes (Figs. 2A–2C) and was consistent between different stimulus sizes. Some activation was also observed in the dorsal V2, but it was never seen in the part of V1 representing the upper visual field or in the ipsilateral V1. The quality of the mappings for the cortical representation of the four ring stimuli of different sizes and of the vertical and horizontal meridians was excellent for all four subjects. Figs. 1 and 2 show typical examples for subject 2. Corresponding results for subjects 3 and 4 are given in Figs. 2 and 5 of our earlier ocular dominance mapping (Cheng et al., 2001).

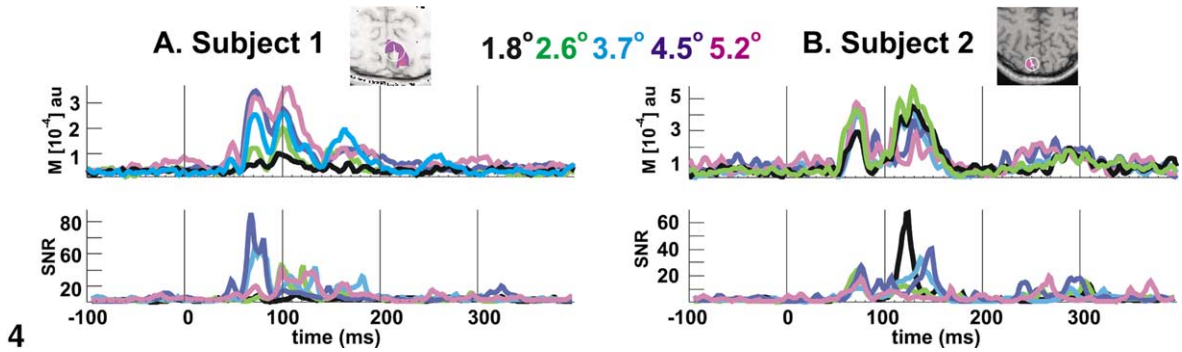

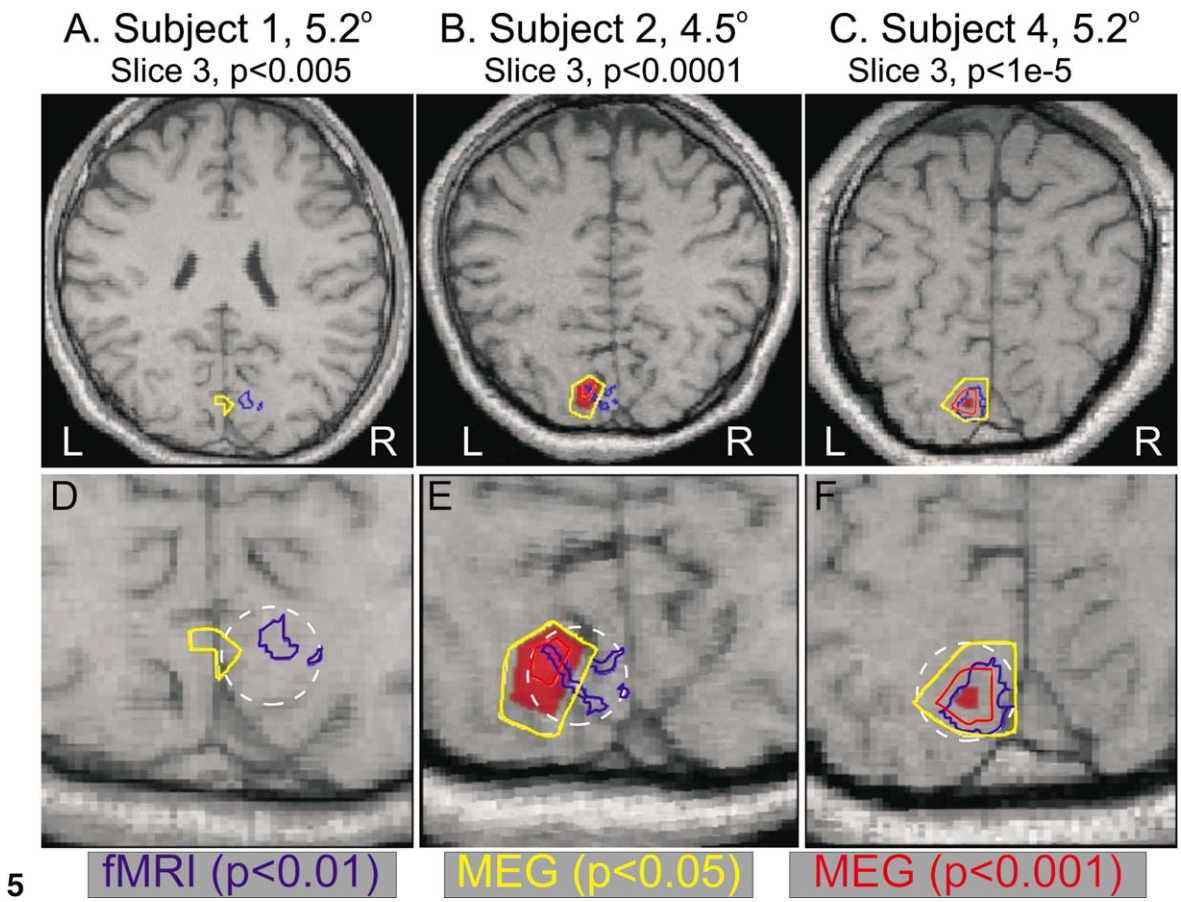

Fig. 4. Activation curves in V1/V2 ROIs for subjects 1 and 2 (top panels) and the corresponding signal to noise ratio (SNR) (lower panels). The activation curves are computed from the modulus of the current density obtained from the MFT solutions. Each color curve represents a stimulus size, which is averaged over the six sets of data for each size (three runs, two patterns in each run).

Fig. 5. Comparison of V1 activation between fMRI and MEG at the onset of M50 (42.4 ms). The results are shown in the paracalcarine slice best covering V1 for subjects 1, 2, and 4 in (A), (B), and (C), respectively. (D–F) Corresponding magnified views of (A–C). In this and Figs. 6 and 7, blue outlines mark the boundary of statistically significant fMRI activations ($P < 0.01$) and white dashed circles mark the estimate for the targeted area. For MEG yellow and red outlines mark the $P < 0.05$ and $P < 0.001$ contours, respectively, and filled red contours denote regions with statistically significant activations within 50% of the peak t value (t_{max}). The P-value corresponding to t_{max} is also printed for each subject.

MEG signal

Fig. 3 shows typical waveforms for subject 1. The amplitude and latency of peaks of the MEG signal were different between subjects, but were reproducible between the two patterns in the same run (Fig. 3A) and were similar across the three runs (Fig. 3B). For the larger stimuli two peaks dominate, one around 70 ms (M70) and the other about 100 ms after the reversal (Fig. 3C). Identifiable but less prominent peaks were seen at 150 and 180 ms after each pattern onset. A sharp but very weak peak was also observed within 50 ms; it is just discernible in most runs in

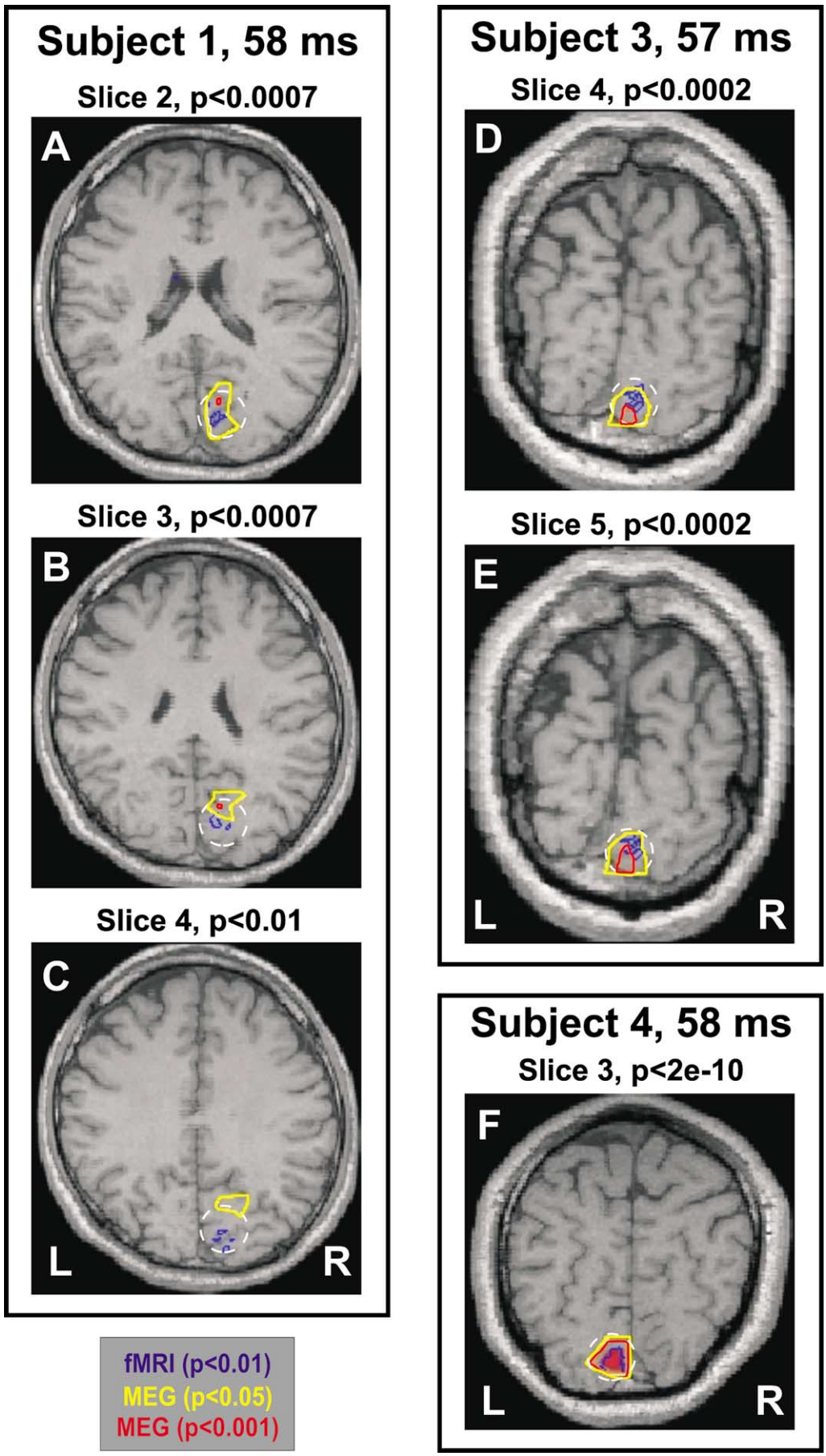

Fig. 6. Comparison of MEG localizations at the onset of the M70 with the fMRI results for the largest stimuli (5.2°) for subjects 1 (A–C), 3 (D, E), and 4 (F). Conventions are the same as for Fig. 5, with the lowest *P* value within each slice printed for each figurine. For subjects 1 and 3 the 50% normalization for the filled red contours is across all slices and corresponds to t_{max} computed across all the displayed slices of the subject.

Table 1
Latency and area of first activation for the M50 and M70 peak

Subject	Stimulus radius (°)	M50			M70		
		Onset *P* value	Onset time	Area(s)	Onset *P* value	Onset time	Area(s)
1	2.6				0.02	66.4	$V1_c/V2_c$
	3.7				$2e^{-7}$	58.4	$V1_c/V2_c$
	4.5				$6e^{-8}$	58.4	$V1_c/V2_c$
	5.2	0.005	42.4	$V1_c$	0.0007	58.4	$V1_c/V2_c/V6_c$
2	2.6				$5e^{-5}$	53.6	$V1_c/V2_c$
	3.7				0.0002	55.2	$V1_c/V2_c$
	4.5	$1e^{-6}$	39.2	$V1_c$	0.001	55.2	$V5_c/V6_c$
	5.2	0.01	36.0	$V2_c/V3_c$	0.02	52.0	$V1_c/V2_c$
3	5.2				0.001	55.2	$V1_c$
4	2.6				0.01	56.8	$V1_c$
	3.7				$5e^{-5}$	61.6	$V1_c/V2_c$
	4.5	0.002	40.8	$V1_c$	0.002	66.4	$V1_c$
	5.2	0.002	39.2	$V1_c$	$1e^{-6}$	56.8	$V1_c$

Note. The assignment to V1 and V2 is made according to the analysis of the preparatory fMRI experiment. The assignment to V5 for subject 3 is from a separate fMRI experiment performed with the same subject. The assignment of V6 follows the results of two recent MEG studies (Tzelepi et al., 2001; Vanni et al., 2001). The subscript c denotes contralateral side to the visual field stimulated.

Fig. 3C. The amplitudes of different components were lower with smaller stimuli, and it was hard to identify evoked responses for radii smaller than 2.6° (Fig. 3C). In general, the amplitude of the M70 component increases with stimulus size.

MFT results

The instantaneous MFT solutions showed peaks in striate and extrastriate regions well within 100 ms. Fig. 4 shows activation time courses computed in a ROI defined around the M70 peak, which covered dorsal V1 and part of V2 on the right hemisphere for subject 1 and on the left hemisphere for subject 2. A weak peak before 50 ms was just discernible for the larger sizes, especially for the largest two stimulus sizes in subject 1. The first consistent change in activity across all sizes was seen just after 50 ms, leading to the M70 peak. The M70 peak value increased from 1.8 to 4.5° for subject 1. For subject 2, the M70 peak increased from 1.8 to 2.6° but remains at about the same level for larger sizes. Note that the highest average signal did not always correspond to the highest SNR, as shown in the lower two panels of the figure.

Post-MFT voxel-by-voxel statistical analysis identified changes in activity that often attained extremely high statistical significance. In all figures showing results of post-MFT statistical analysis we marked with filled red contour statistically significant increases in activity with *t*-values higher than half the maximum *t*-value across the displayed slices, provided the corresponding *P*-values were still higher than 0.05. To maintain consistency across activations and similarity in representation between fMRI and MEG we also marked post-MFT activity increases with *P* values of 0.05 and 0.001 using yellow and red outlines, respectively. For each subject significant change in activity was detected at latencies well within the M70 peak. Significant change in V1 activation was observed at the beginning of waves of activity, followed by activity in other areas outside V1. The first such wave started close to 40 ms after the stimulus onset and ended by 50 ms, which we referred to as M50. Table 1 lists the times and loci of the first significant activations at the onset of the M50 and M70. At the onset of M50, statistically significant activity in V1 was identified for at least one of the two larger sizes (4.5 and/or 5.2°) in three subjects (1, 2, and 4). Fig. 5 shows that these early V1 activations were very focal and in excellent agreement with the fMRI V1 localization. At the onset of the M70, the V1 activation was identified in three subjects (1, 2, and 4) for sizes from 2.6° and larger, spreading within a few milliseconds to other areas. For subject 3, the V1 activation at the onset of M70 was observed only for the largest stimulus (5.2°). For most subjects and sizes, the first significant V1 activation at the onset of M70 was between 50 and 60 ms. Fig. 6 shows the first significant V1 activations for the largest stimulus size (5.2°) at the onset of M70 for subjects 1, 3, and 4. The rapid involvement of other areas at the onset of M70 is demonstrated in Fig. 7A for subject 2 with stimulus size 3.7°. Fig. 7B shows recruitment of new areas as the size of the stimulus changes for the same subject (subject 2). For the smaller stimuli (2.7 and 3.7°) the early M70 onset is restricted to the V1/V2 area, but for the larger sizes either other areas become activated very early, masking the V1 activation (4.5°), or the V1/V2 activation is seen briefly (if at all) just a few milliseconds earlier (5.2°). In Fig. 7, the activations corresponding to the putative V6 homologue and V5 (determined in a separate fMRI experiment for the same subject) are also highlighted.

Visual inspection of the solutions shows that the agree-

Table 2
Loci and center-to-center distance between fMRI and MEG localizations

Subject	Time (ms)	Targeted area			FMRI (for $P < 0.001$) (for $P < 0.005$)			MEG			Distance (mm)
		x (mm)	y (mm)	z (mm)	x (mm)	y (mm)	z (mm)	x (mm)	y (mm)	z (mm)	
1	42.4	9.5	−87.5	1.5	10.4	−80.2	6.3	1.1	−83.1	5.9	9.75
					1.3	−82.0	3.7				2.47
2	42.4	−5.5	−98.0	1.5	−9.2	−89.0	1.6	−10.1	−89.3	0.7	1.31
					−8.2	−90.4	1.0				2.22
3	56.8	3.5	−82.0	7.0	3.4	−81.8	4.1	1.1	−84.7	−0.9	6.22
					4.5	−85.1	3.4				5.50
4	42.4	−9.0	−80.0	4.0	−7.7	−82.8	1.1	−9.8	−81.8	2.2	2.57
					−8.8	−82.8				1.79	
Mean											4.96
											3.00
SD											3.81
											1.69

Note. Talairach coordinates of the centers of the targeted areas for the fMRI and MEG activations. The last column shows the distance between the centers of the fMRI and MEG loci. Two estimates are used for fMRI activations, corresponding to $P < 0.001$ and $P < 0.005$, respectively.

ment between the fMRI and MEG estimates of *early* V1 activation is excellent. It is difficult to objectively reduce the comparison between the time-varying activations of MEG with the single fMRI activation to just one number. We nevertheless computed the distance between the centers of the two best estimates for the sake of a more quantitative measure. The results are given in Table 2, with the coordinates transformed into the standard Talairach space, to make it easy to compare the loci of activity across subjects. For MEG we used the center of the contour for the first statistically significant activation from one of the two larger sizes for MEG (i.e., the activations in Fig. 5 for subjects 1, 2, and 4 and in Fig. 6 for subject 3). For fMRI we used the center of the V1 contour, computed with $P < 0.01$ and $P < 0.05$ (top and bottom rows in Table 2 for each subject). For subjects 1 and 2 where more than one such contours were present we selected the one closest to the MEG activation. The results were very similar for the two thresholds except for subject 1, where the lower threshold ($P < 0.05$) produced a new small activation close to the midline and improved the comparison between fMRI and MEG centers of activity dramatically (from 9.8 to 2.5 mm). The mean mismatch for the localization between fMRI and MFT results is 5 ($\pm$3.8) mm and 3 ($\pm$1.7) mm for the fMRI activations with $P < 0.01$ and $P < 0.05$, respectively.

fMRI postscript

Fig. 8 shows the results of a repeated fMRI experiment for subject 2, contrasting the localization for the two flickering frequencies (0.71 and 8 Hz) and the localization for the first and second repetition of the fMRI experiment (8 Hz). The activated area within V1 is almost indistinguishable between the two flickering frequencies and between the first and the second experiment. This remarkable demonstration of the expected accuracy of our fMRI localization confirms the suitability of our protocol choice for V1 activation as a gold standard for testing MEG localization.

Discussion

In our earlier MEG study (Tzelepi et al., 2001) we demonstrated that using MFT localization with accurate retinotopy is possible from relatively small number of trials with stimuli large sinusoidal spatial gratings with MFT. To test for higher resolution we needed to use smaller stimuli and a more precise comparison standard. Our earlier fMRI studies showed that such a standard could be provided by high-field fMRI (Cheng et al., 2001). In designing the experiment we were guided by neurophysiology and anatomy and the need to minimize problems at the technical level for each technique.

Superficial potentials and evoked magnetic fields outside the head depend on the morphology of the cortical sulci and gyri, alignment of pyramidal cells, and extent and nature of intracortical and cortico-cortical connections (Nunez and Silberstein, 2000). The activity from nearby areas could be difficult to resolve from the MEG signal when the net electrical current in each area flows in roughly the same direction. In the opposite extreme the net MEG signal could be very small if the electrical current in two nearby active areas flows in roughly the opposite direction. It is therefore desirable to confine the excited area to just one part of the main cytoarchitectonic area to be investigated with no sharp surface normal changes. It is impossible in a noninvasive experiment to activate just one cytoarchitectonic area, so the best one can do is to keep the targeted area as far away as possible from other cytoarchitectonic areas which may also be excited by the stimulus. These considerations led us to

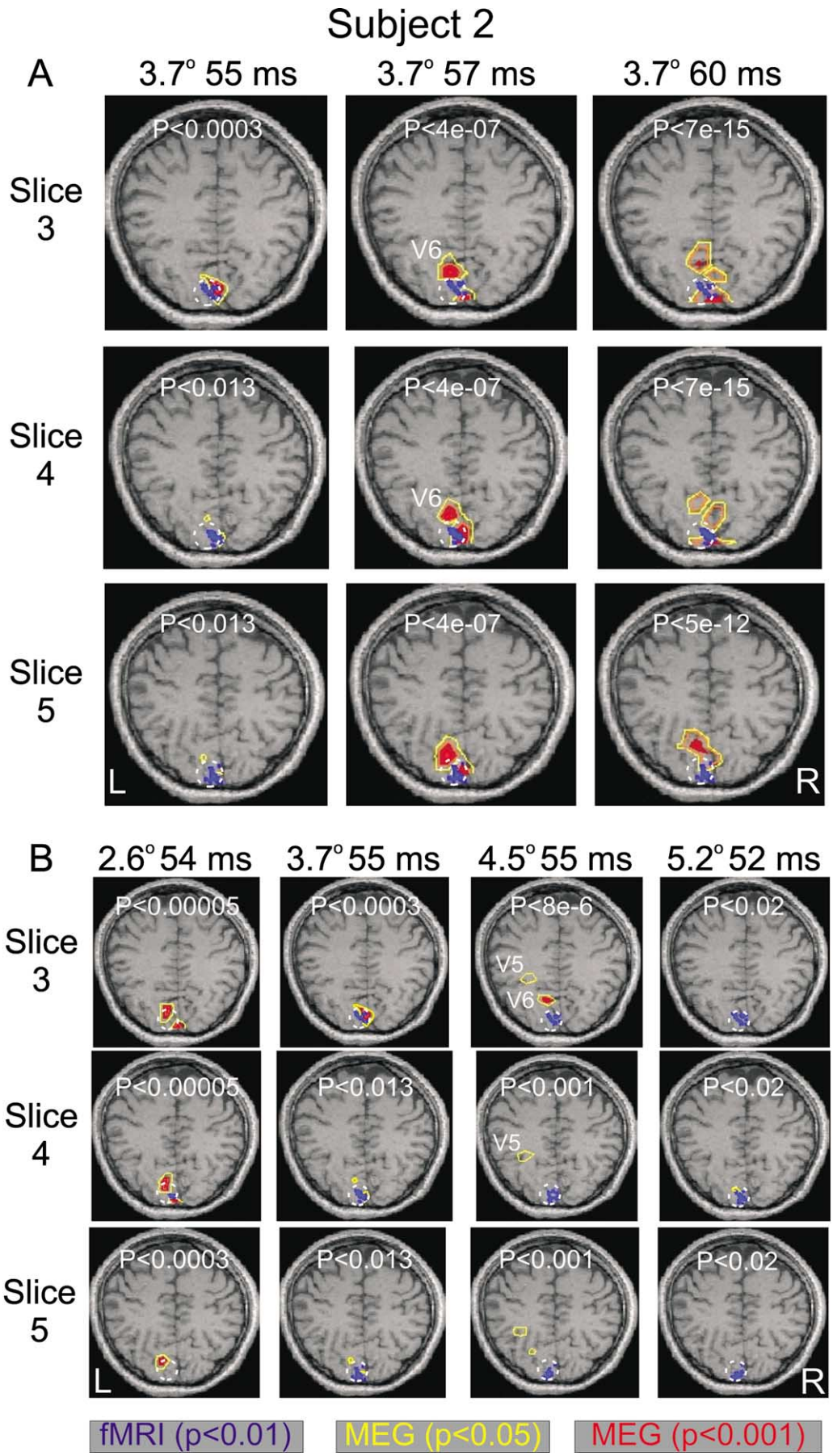

Fig. 7. Comparison of loci of significant change of activity at the very beginning of the M70 for subject 2 between fMRI and MEG. (A) Changes as a function of time (column) shown in three slices (row) for stimulus size 3.7°. (B) Changes as a function of stimulus size (column) shown in three slices. The three slices displayed are the ones shown to contain V1, marked as slices 3, 4, and 5 in Fig. 1A. Conventions are the same as for Fig. 5, with the lowest *P* value shown for each figurine separately. For each time slice and size the normalization for the filled red contours is across the three displayed levels.

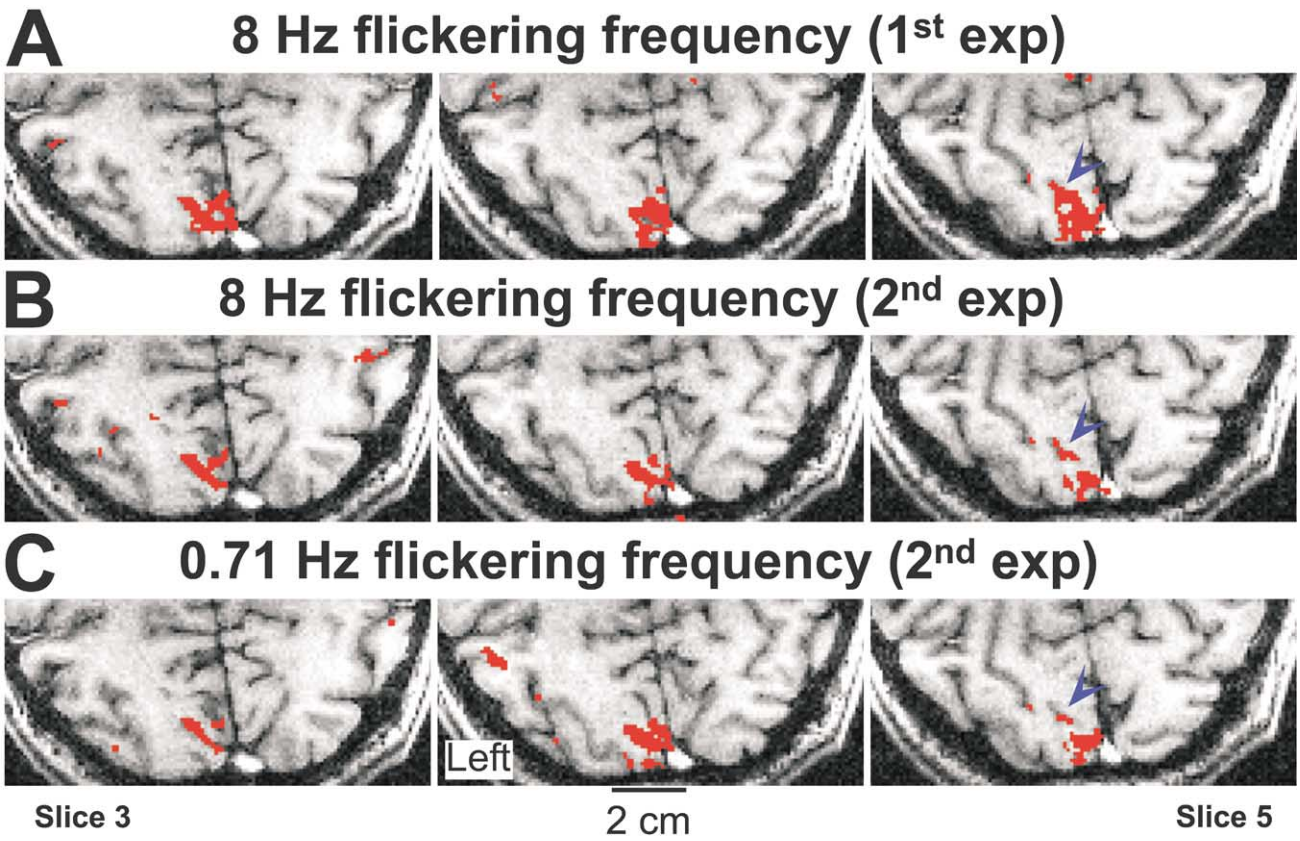

Fig. 8. Independence of fMRI activation on the flickering frequency and reproducibility of activation in two different fMRI experiments (16 months apart) for subject 2. For all parts of the figure the stimulus was the flickering checkerboard with radius 4.5° placed at eccentricity of 8° on the lower right quadrant of the visual field. The prescription of slices in the two separate fMRI experiments ((A) first; (B, C) second experiment) was almost identical producing activation in V1 in the same three slices (3, 4 and 5) of the six-slice volume covered. These slices are the same as the ones displayed in Fig. 2 and used again here for consistency. (A) Results of the first experiment (flickering frequency at 8 Hz) but just for the stimulus of radius 4.5°. (B) Results of the second experiment with the flickering frequency at 8 Hz. (C) Results of the new experiment with the flickering frequency used in the MEG experiment (0.71 Hz). All maps were generated at $P < 0.01$. The blue arrows indicate the activation in V2.

restrict the stimulus to the center of a quadrant of the visual field. The targeted quadrant was chosen according to the morphology around the calcarine sulcus of each subject, so that the estimated center of the activated area in V1 lay well below the dorsal V1/V2 border to minimize interference from V2, and away from the fundus of the calcarine sulcus. With this choice, presenting a stimulus in a small area of the visual field should excite a cortical patch reasonably well approximated by its local tangent plane, hence avoiding large-scale cancellations of the external magnetic field because of nonuniformity in the current density distribution. However, SNR decreases as the activated area becomes smaller. Since the optimal size is difficult to estimate in advance, we varied systematically the stimulus size while keeping its center fixed.

The fMRI localization is uniquely defined by the data and is limited primarily by noise. Therefore, leaving aside the questions of hemodynamic delay and large vessel artifacts (which are not major problem for our experiment), the fMRI loci of significant change, backed by the a priori prediction of the retinotopic mapping experiment, provides as close to a “gold standard” measure as is available today. In fMRI experiments, macrovascular changes distal to the site of the actual neuronal activity may occur and even mask the BOLD signal coming from microvasculature. This technical problem is reduced at high magnetic fields. The BOLD response dependence on the external magnetic field changes with the blood vessel size. For small blood vessels the dependence is quadratic but for large ones it is linear, and it has been shown that at least up to 4 T, the contrast to noise ratio increases with the magnetic field (Ogawa et al., 1998; Ugurbil et al., 1999). To reduce any residual effect due to large venous vessels, voxels with average signal change above 10%, which are known to be associated with large vessels, were discarded (Cheng et al., 2001; Gati et al., 1997; Luh et al., 2000). Motion reduction strategies also help in reliable localization of cortical activations using fMRI.

With the steps described above, the present study demonstrated consistent and accurate localization of V1 activity with MEG and fMRI tomographic statistical maps following precise visual stimulation. The accuracy of just a few millimeters reported here is almost an order of magnitude better than most previously reported comparisons of fMRI

and MEG localization. Two other conclusions follow from our results. First, focal activity from V1 can be identified from the MEG data as early as 40 ms after stimulus onset, consistent with the early striate activation reported for neurons in layer 4C in monkey (Maunsell and Gibson, 1992; Schmolesky et al., 1998). Second, the M70 wave begins with an early activation of V1 which is followed within a few milliseconds by activity in other areas, including human homologues of V5 and putative V6.

The evidence from electrode recording in monkeys supports both the early V1 activation and an overlap of the V1 time course with that of V2 and other areas. Many neurons in V1 and V2 activate simultaneously (Nowak et al., 1995, 1999). Extensive overlap has been found between activity of V1, V2, and V5, with median latencies for V2 and V5 about 10 ms later than V1 in macaque (Raiguel et al. 1989). Also, activity in V3, MST, and FEF appears less than 10 ms after the V1 response (Schmolesky et al., 1998), and it takes as little as 23 ms for V1 to activate the inferotemporal cortex (Schroeder et al., 1998). Findings in monkeys do not necessarily hold for humans, but it is likely that the spread of activity through the human visual system would also be very fast, as recently suggested by EEG data analysis (Foxe and Simpson, 2002). Single trials with similar activity in primary sensory areas at the onset of each wave of activation may proceed in different ways in higher areas, as we have recently shown to be the case in the somatosensory system (Ioannides et al., 2002).

This puts a different perspective on the M70 and its EEG analogue the N70 (Bodis-Wollner et al., 1981) which were previously considered to represent V1 activity alone (Hillyard and Anllo-Vento, 1998; Martinez et al., 1999). Our results agree with recent MEG and EEG studies in humans showing early activation in occipitotemporal (Buchner et al., 1997; Ffytche et al., 1995; Tzelepi et al., 2001) and parietooccipital (Clark et al., 1995; Tzelepi et al., 2001; Vanni et al., 2001) regions, and the more recent scalp current density analysis (Foxe and Simpson, 2002).

In summary, MFT solutions identified activations in many extrastriate areas soon after the V1 activation. The work presented here demonstrates that the localization accuracy of MEG with MFT, at least at the level of V1, is within a few millimeters of the fMRI loci. Good localization might indeed be possible in extrastriate areas with more cognitive scenarios, especially from post-MFT analysis of single-trial MFT solutions, as has been recently demonstrated in a number of studies (Ioannides, 2001).

References

Ahlfors, S.P., Ilmoniemi, R.J., Hamalainen, M.S., 1992. Estimates of visually evoked cortical currents. Electroencephalogr. Clin. Neurophysiol. 82, 225–236.

Aine, C.J., Supek, S., George, J.S., Ranken, D., Lewine, J., Sanders, J., Best, E., Tiee, W., Flynn, E.R., Wood, C.C., 1996. Retinotopic organization of human visual cortex: departures from the classical model. Cereb. Cortex 6, 354–361.

Beisteiner, R., Erdler, M., Teichtmeister, C., Diemling, M., Moser, E., Edward, V., Deecke, L., 1997. Magnetoencephalography may help to improve functional MRI brain mapping. Eur. J. Neurosci. 9, 1072–1077.

Bodis-Wollner, I., Barris, M., Mylin, L., Julesz, B., Kropfl, W., 1981. Binocular stimulation reveals cortical components of the human visual evoked potential. Electroenceph. Clin. Neurophysiol. 52, 298–305.

Bonmassar, G., Schwartz, D.P., Liu, A.K., Kwong, K.K., Dale, A.M., Belliveau, J.W., 2001. Spatiotemporal brain imaging of visual-evoked activity using interleaved EEG and fMRI recordings. NeuroImage 13, 1035–1043.

Buchner, H., Gobbele, R., Wagner, M., Fuchs, M., Waberski, T.D., Beckmann, R., 1997. Fast visual evoked potential input into human area V5. NeuroReport 8, 2419–2422.

Cheng, K., Waggoner, R.A., Tanaka, K., 2001. Human ocular dominance columns as revealed by high-field functional magnetic resonance imaging. Neuron 32, 359–374.

Clark, V.P., Fan, S., Hillyard, S.A., 1995. Identification of early visual evoked potential generators by retinotopic and topographic analysis. Human Brain Mapping 2, 170–187.

DeYoe, E.A., Carman, G.J., Bandettini, P., Glickman, S., Wieser, J., Cox, R., Miller, D., Neitz, J., 1996. Mapping straite and extrastriate visual areas in human cerebral cortex. Proc. Natl. Acad. Sci. USA 93, 2382–2386.

Disbrow, E.A., Slutsky, D.A., Roberts, T.P., Krubitzer, L.A., 2000. Functional MRI at 1.5 tesla: a comparison of the blood oxygenation level-dependent signal and electrophysiology. Proc. Natl. Acad. Sci. USA 97, 9718–9723.

Engel, S.A., Glover, G.H., Wandell, B.A., 1997. Retinotopic organization in human visual cortex and the spatial precision of functional MRI. Cereb. Cortex 7, 181–192.

Eulitz, C., Elbert, T., Bartenstein, P., Weiller, C., Muller, S.P., Pantev, C., 1994. Comparison of magnetic and metabolic brain activity during a verb generation task. NeuroReport 6, 97–100.

Ffytche, D.H., Guy, C.N., Zeki, S., 1995. The parallel visual motion inputs into areas V1 and V5 of human cerebral cortex. Brain 118, 1375–1394.

Fox, P.T., Miezin, F.M., Allman, J.M., Van Essen, D.C., Raichle, M.E., 1987. Retinotopic organization of human visual cortex mapped with positron-emission tomography. J. Neurosci. 7, 913–922.

Foxe, J.J., Simpson, G.V., 2002. Flow of activation from V1 to frontal cortex in humans. A framework for defining early visual processing. Exp. Brain. Res. 142, 139–150.

Galletti, C., Fattori, P., Gamberini, M., Kutz, D.F., 1999. The cortical visual area V6: brain location and visual topography. Eur. J. Neurosci. 11, 3922–3936.

Gati, J.S., Menon, R.S., Ugurbil, K., Rutt, B.K., 1997. Experimental determination of the BOLD field strength dependence in vessels and tissue. Magn. Reson. Med. 38, 296–302.

Gratton, G., Fabiani, M., Corballis, P.M., Hood, D.C., Goodman-Wood, M.R., Hirsch, J., Kim, K., Friedman, D., Gratton, E., 1997. Fast and localized event-related optical signals (EROS) in the human occipital cortex: comparisons with the visual evoked potential and fMRI. NeuroImage 6, 168–180.

Hamalainen, M., Hari, R., Ilmoniemi, R.J., Knuutila, J., Lounasmaa, O.V., 1993. Magnetoencephalography—theory, instrumentation, and applications to noninvasive studies of the working human brain. Rev. Mod. Phys. 65, 413–497.

Hillyard, S.A., Anllo-Vento, L., 1998. Event-related brain potentials in the study of visual selective attention. Proc. Natl. Acad. Sci. USA 95, 781–787.

Horton, J.C., Hoyt, W.F., 1991. The representation of the visual field in human striate cortex. A revision of the classic Holmes map. Arch. Ophthalmol. 109, 816–824.

Hu, X., Kim, S.G., 1994. Reduction of signal fluctuation in functional MRI using navigator echoes. Magn. Reson. Med. 31, 495–503.

Hu, X., Le, T.H., Parrish, T., Erhard, P., 1995. Retrospective estimation and correction of physiological fluctuation in functional MRI. Magn. Reson. Med. 34, 201–212.

Ioannides, A.A., 1994. Estimation of brain activity using magnetic field tomography and large scale communication within the brain, in: Ho, M.W., Popp, F.A., Warnke, U. (Eds.), Bioelectronics and Biocommunication, World Scientific, Singapore, pp. 319–353.

Ioannides, A.A., 1999. Problems associated with the combination of MEG and fMRI data: theoretical basis and results in practice, in: Yoshimoto, T., Kotani, M., Kuriki, S., Karibe, H., Nakasato, N. (Eds.), Recent Advances in Biomagnetism, Tohoku Univ. Press, Sendai, pp. 133–136.

Ioannides, A.A., 2001. Real time human brain function: observations and inferences from single trial analysis of magnetoencephalographic signals. Clinical EEG 32, 98–111.

Ioannides, A.A., Bolton, J.P.R., Clarke, C.J.S., 1990. Continuous probabilistic solutions to the biomagnetic inverse problem. Inverse Probl. 6, 523–542.

Ioannides, A.A., Kostopoulos, G.K., Laskaris, N.A., Liu, L.C., Shibata, T., Schellens, M., Poghosyan, V., Khurshudyan, A., 2002. Timing and connectivity in the human somatosensory cortex from single trial mass electrical activity. Human Brain Mapping 15, 231–246.

Ioannides, A.A., Muratore, R., Balish, M., Sato, S., 1993a. In vivo validation of distributed source solutions for the biomagnetic inverse problem. Brain Topogr. 5, 263–273.

Ioannides, A.A., Singh, K.D., Hasson, R., Baumann, S.B., Rogers, R.L., Guinto, F.C., Papanicolaou, A.C., 1993b. Comparison of current dipole and magnetic field tomography analyses of the cortical response to auditory stimuli. Brain Topogr. 6, 27–34.

Kim, D.S., Duong, T.Q., Kim, S.G., 2000. High-resolution mapping of iso-orientation columns by fMRI. Nat. Neurosci. 3, 164–169.

Luh, W.M., Wong, E.C., Bandettini, P.A., Ward, B.D., Hyde, J.S., 2000. Comparison of simultaneously measured perfusion and BOLD signal increases during brain activation with T_1-based tissue identification. Magn. Reson. Med. 44, 137–143.

Maas, L.C., Frederick, B.D., Renshaw, P.F., 1997. Decoupled automated rotational and translational registration for functional MRI time series data: the DART registration algorithm. Magn. Reson. Med. 37, 131–139.

Maclin, E., Okada, Y., Kaufman, L., Williamson, S.J., 1983. Retinotopic map on the visual cortex for eccentrically placed patterns: first noninvasive measurement. Nuovo Cimento 2D, 410–419.

Martinez, A., Anllo-Vento, L., Sereno, M.I., Frank, L.R., Buxton, R.B., Dubowitz, D.J., Wong, E.C., Hinrichs, H., Heinze, H.J., Hillyard, S.A., 1999. Involvement of striate and extrastriate visual cortical areas in spatial attention. Nat. Neurosci. 2, 364–369.

Maunsell, J.H., Gibson, J.R., 1992. Visual response latencies in striate cortex of the macaque monkey. J. Neurophysiol. 77, 1332–1344.

Menon, R.S., Goodyear, B.G., 1999. Submillimeter functional localization in human striate cortex using BOLD contrast at 4 Tesla: implications for the vascular point-spread function. Magn. Reson. Med. 41, 230–235.

Menon, R.S., Ogawa, S., Strupp, J.P., Ugurbil, K., 1997. Ocular dominance in human V1 demonstrated by functional magnetic resonance imaging. J. Neurophysiol. 77, 2780–2787.

Nakamura, A., Kakigi, R., Hoshiyama, M., Koyama, S., Kitamura, Y., Shimojo, M., 1997. Visual evoked cortical magnetic fields to pattern reversal stimulation. Brain Res. Cogn. Brain Res. 6, 9–22.

Nowak, L.G., Munk, M.H., Girard, P., Bullier, J., 1995. Visual latencies in areas V1 and V2 of the macaque monkey. Vis. Neurosci. 12, 371–384.

Nowak, L.G., Munk, M.H., James, A.C., Girard, P., Bullier, J., 1999. Cross-correlation study of the temporal interactions between areas V1 and V2 of the macaque monkey. J. Neurophysiol. 81, 1057–1074.

Nunez, P.L., Silberstein, R.B., 2000. On the relationship of synaptic activity to macroscopic measurements: does co-registration of EEG with fMRI make sense? Brain Topogr. 13, 79–96.

Ogawa, S., Menon, R.S., Kim, S.G., Ugurbil, K., 1998. On the characteristics of functional magnetic resonance imaging of the brain. Annu. Rev. Biophys. Biomol. Struct. 27, 447–474.

Okada, Y., 1983. Neurogenesis of evoked magnetic fields, in: Williamson, S.J., Romani, G., Kaufman, L., Modena, I. (Eds.), Biomagnetism: An Interdisciplinary Approach, Plenum, New York, pp. 399–421.

Onofrj, M., Fulgente, T., Thomas, A., Curatola, L., Peresson, M., Lopez, L., Locatelli, T., Martinelli, V., Comi, G., 1995. Visual evoked potentials generator model derived from different spatial frequency stimuli of visual field regions and magnetic resonance imaging coordinates of V1, V2, V3 areas in man. Int. J. Neurosci. 83, 213–239.

Portin, K., Vanni, S., Virsu, V., Hari, R., 1999. Stronger occipital cortical activation to lower than upper visual field stimuli. Exp. Brain Res. 124, 287–294.

Raiguel, S.E., Lagae, L., Gulyas, B., Orban, G.A., 1989. Response latencies of visual cells in macaque areas V1, V2 and V5. Brain Res. 493, 155–159.

Ribary, U., Ioannides, A.A., Hasson, R., Singh, K.D., Bolton, J.P.R., Lado, F., Mogilner, A., Llinas, R., 1991. Magnetic field tomography (MFT) of coherent thalamo-cortical 40 Hz oscillations in humans. Proc. Nat. Acad. Sci. USA 88, 11037–11041.

Roberts, T.P., Disbrow, E.A., Roberts, H.C., Rowley, H.A., 2000. Quantification and reproducibility of tracking cortical extent of activation by use of functional MR imaging and magnetoencephalography. Am. J. Neuroradiol. 21, 1377–1387.

Rosen, B.R., Buckner, R.L., Dale, A.M., 1998. Event-related functional MRI: past, present, and future. Proc. Natl. Acad. Sci. USA 95, 773–780.

Schmolesky, M.T., Wang, Y., Hanes, D.P., Thompson, K.G., Leutgeb, S., Schall, J.D., Leventhal, A.G., 1998. Signal timing across the macaque visual system. J. Neurophysiol. 79, 3272–3278.

Schroeder, C.E., Mehta, A.D., Givre, S.J., 1998. A spatiotemporal profile of visual system activation revealed by current source density analysis in the awake macaque. Cereb. Cortex 8, 575–592.

Sereno, M.I., Dale, A.M., Reppas, J.B., Kwong, K.K., Belliveau, J.W., Brady, T.J., Rosen, B.R., Tootell, R.B., 1995. Borders of multiple visual areas in humans revealed by functional magnetic resonance imaging. Science 268, 889–893.

Singh, K.D., Smith, A.T., Greenlee, M.W., 2000. Spatiotemporal frequency and direction sensitivities of human visual areas measured using fMRI. NeuroImage 12, 550–564.

Slotnick, S.D., Klein, S.A., Carney, T., Sutter, E., Dastmalchi, S., 1999. Using multi-stimulus VEP source localization to obtain a retinotopic map of human primary visual cortex. Clin. Neurophysiol. 110, 1793–1800.

Stippich, C., Freitag, P., Kassubek, J., Soros, P., Kamada, K., Kober, H., Scheffler, K., Hopfengartner, R., Bilecen, D., Radu, E.W., Vieth, J.B., 1998. Motor, somatosensory and auditory cortex localization by fMRI and MEG. NeuroReport 9, 1953–1957.

Strupp, J.P., 1996. Stimulate: a GUI based fMRI analysis software package. NeuroImage 3, S607.

Taylor, J.G., Ioannides, A.A., Müller-Gärtner, H.W., 1999. Mathematical analysis of lead field expansions. IEEE Trans. Med. Imag. 18, 151–163.

Thomas, C.G., Menon, R.S., 1998. Amplitude response and stimulus presentation frequency response of human primary visual cortex using BOLD EPI at 4 T. Magn. Reson. Med. 40, 203–209.

Tzelepi, A., Ioannides, A.A., Poghosyan, V., 2001. Early (N70m) neuromagnetic signal topography and striate and extrastriate generators following pattern onset quadrant stimulation. NeuroImage 13, 702–718.

Ugurbil, K., Hu, X., Chen, W., Zhu, X.H., Kim, S.G., Georgopoulos, A., 1999. Functional mapping in the human brain using high magnetic fields. Philos. Trans. R. Soc. Lond. B Biol. Sci. 354, 1195–1213.

Vanni, S., Tanskanen, T., Seppa, M., Uutela, K., Hari, R., 2001. Coinciding early activation of the human primary visual cortex and anteromedial cuneus. Proc. Natl. Acad. Sci. USA 98, 2776–2780.